Thermophysical properties of water ethylene glycol (WEG) mixture-based Fe3O4 nanofluids at low concentration and temperature

Alireza Banisharif, Masoud Aghajani, Stephan van Vaerenbergh, Patrice Estellé, Alimorad Rashidi

Thermophysical Properties of Water Ethylene Glycol (WEG) Mixture-based Fe_3O_4 Nanofluids at low Concentration and Temperature

Alireza Banisharif[1,2], **Masoud Aghajani**[1,*], **Stephan Van Vaerenbergh**[2], **Patrice Estellé**[3,*] **and Alimorad Rashidi**[4]

[1] Gas Engineering Department, Petroleum University of Technology, Ahwaz, Iran

[2] Chimie-Physique (MRC), Université Libre de Bruxelles, 1050, Brussels, Belgium

[3] Univ Rennes, LGCGM, EA3913, 35704 Rennes, France

[4] Nanotechnology Research Centre, Research Institute of Petroleum Industry (RIPI), Tehran, Iran

[*]Corresponding authors: patrice.estelle@univ-rennes1.fr; m.aghajani@put.ac.ir

Abstract

In the present work, Fe_3O_4 nanoparticles produced by the ultrasonic precipitation method and characterized by XRD, SEM, and BET methods are used to produce nanofluids using a mixture of water and ethylene glycol (WEG 50:50) as a base fluid and both sodium dodecyl sulfonate and oleic acid as surfactants. The thermal conductivity, dynamic viscosity and surface tension of these Fe_3O_4 nanofluids are experimentally evaluated for temperatures ranging from 253.15 to 293.15K and different volume concentrations of nanoparticles, 0.01, 0.05 and 0.1% respectively. Experiments indicate that the thermophysical properties of nanofluids are strongly dependant on concentrations of nanoparticles and temperatures, particularly at sub-zero temperatures. Actually, it is shown that the thermal conductivity of nanofluids increases with almost 9.5%, and 14.3%, at 263.15K and 293.15K respectively, with 0.1 vol%. The thermal conductivity enhancement of nanofluids with concentration and temperature is compared to some relevant theoretical models. A good agreement is achieved with a comprehensive model taking into consideration effective medium theory, the nanolayer effect of molecules around the solid particle, Brownian motion of nanoparticles encompassing aggregation and nano-convection. It is also found that the dynamic viscosity of nanofluids decreases with nanoparticle content in particular below

273.15K, up to 40% at 0.1% in volume. Surface tension decreases by adding the surfactant to the base fluid and then increases with Fe_3O_4 concentration with nearly 38% and 33% with 0.1% in nanoparticle volume fraction at 253.15 and 293.15K, respectively. Finally, these results are promising in view of Fe_3O_4 nanofluids use in cooling applications.

Keywords: Fe_3O_4 nanofluids, low and sub-zero temperatures, Thermal conductivity, Viscosity, Surface tension

1. Introduction

Nanofluids, now well-known as suspended nanoparticles in molecular liquids, are promising thermal liquids, because of their thermal transfer properties that are generally significantly better than base fluids [1]. Water, ethylene glycol, propylene glycol, engine oil, and refrigerants are commonly used in literature as base fluids. Nanofluids have special properties that make them conceivably valuable in many applications, such as microelectronics, engine transmission oil, refrigeration, drilling, lubrication, thermal storage, the improved heat transfer efficiency of chillers, engine cooling and hybrid-powered engines, domestic refrigerator-freezers, machining cooling, nuclear reactor, pharmaceutical processes, etc [2]. Nanofluid thermal conductivities are usually higher than the ones of base fluid and the enhancement is linked to nanoparticle content, size, shape, nature… However, this is also generally coupled to viscosity enhancement that is detrimental in view of practical perspectives. Among all nanofluids, Fe_3O_4 nanofluids have great potential applications, because of unique magnetic properties that can be combined to thermal efficiency. Basically, Fe_3O_4 oil-based nanofluids were introduced by Akoh et al. [3]. Use of magnetic fluids for heat transfer applications has been reported previously in [3-5]. Li et al. [6] investigated the viscosity and the thermal conductivity of Fe_3O_4 nanoparticles dispersed in water-based fluid with a volume fraction from 1% to 5% wt. at 293.15 K. The impact of agglomeration and alignment of nanoparticles on the thermal physical properties of Fe_3O_4 nanofluids in the volume fraction range of 0.5-5% have been studied by Zhu et al [7]. The outcomes demonstrated that Fe_3O_4 nanofluids from have higher thermal conductivities than various compound aqueous nanofluids at room temperature. They found that even at the volume fraction of 0.005 the thermal conductivity ratios increased by more than 15.0 percent. In wider context, the open literature shows that most researches have been

performed at intermediate and high temperatures in particular to enhance the rate of heat transfer in heating applications. The use of nanofluids and their marketing in cooling industrial applications is still limited due to the weak development of nanofluid research at low temperatures [8]. Aladag et al. [9] studied Al_2O_3 and CNT water-based nanofluids at small concentrations for a range of temperatures from 271.15 to 283.15K. Experiments demonstrated that the nanofluids behaved as either Newtonian or non-Newtonian fluids, based on the shear rate. Halelfadl et al. [10] reported the steady-state dynamic viscosity of water-based nanofluids based on multi-walled carbon nanotubes, taking into account the influence of particle volume fraction (0.0055% and 0.55%) and temperature from 273.15 to 313.15K. Nanofluids behaved as shear-thinning materials for high particle content while the nanofluids are rather Newtonian for lower particle content. Water with ethylene glycol or polyethylene glycol are usually used as a base fluid at low temperature because of the low freezing point of water. Some researchers used water/ethylene glycol and water/propylene glycol mixtures as a base fluids for nanofluid preparation. Numburu et al. [11] studied the viscosity CuO nanofluid for 40:60% of W/EG mixture in the temperature range from 238.15 to 323.15K. Kulkarni et al. [11-13] studied the effect of low temperature on viscosity of CuO, SiO_2, and Al_2O_3 Water/Ethylene Glycol-based nanofluids in the same temperature range. Their results indicate that for higher temperatures, the nanofluids behave as Newtonian fluids and for lower temperature, a shear-thinning behaviour was obtained. They indicated that with the increase in temperature, the viscosity reduces exponentially. Naik et al. [14] measured the viscosity of CuO nanoparticles into water and propylene glycol (40:60 by weight) with different particle volume concentration of 0.025 to 1.2% at temperatures between 258.15 and 303.15K. They noted an exponential increase in viscosity as temperature decreases. Υ-Fe_2O_3 nanoparticles with different volume fractions from 0.005 to 0.02 were considered by Guo et al. [15] to produce nanofluids with a mixture of water and ethylene glycol with volume ratio of 55:45 in the temperature range from 263.15 to 333.15K. Sundar et al. [16] investigated the viscosity measurement of Fe_3O_4 nanoparticles dispersed in water/ethylene glycol mixture at concentrations ranging from 0 to 1.0 volume percent, the temperature range varying from 273.15 to 323.15K. It was shown that nanofluid viscosity rises with volume concentration and decreases with temperature. Naik and Sundar [17] also prepared CuO nanofluid with a water/propylene glycol mixture (30:70%) as base fluid and noticed thermal conductivity enhancements of 10.9% and

43.37% for 1.2 vol% and at 298.15 and 338.15K, respectively. Their results also indicated that the thermal conductivity of CuO nanofluids is improved with the increase in the concentration of CuO nanoparticles. Sunder et al. [18] also investigated the thermal conductivity and viscosity of Fe_3O_4 nanoparticles into 20:80% and 40:60% of propylene glycol and water mixture as based fluids in the temperatures of 273.15 and 333.15K. Results show that the nanofluid thermal conductivity increases with nanoparticle content and temperature. Nanofluid viscosity also increases with concentrations of nanoparticles. The rheological measurements between 263.15 and 313.15K for TiO_2 nanoparticle dispersions in polyethylene glycol were also reported by Yapici et al [19].

In summary, this short literature overview shows that the thermophysical properties of nanofluids are still rarely investigated at low and sub-zero temperatures (in °C), in particular using Fe_3O_4 nanoparticles that are considered as emerging and promising candidates for nanofluid applications. Therefore, the aim of this paper is to investigate the thermophysical properties of Fe_3O_4 nanofluids such as the thermal conductivity, viscosity and surface tension. The nanofluids are presently produced with Water-Ethylene Glycol mixture (WEG 50:50 by volume at 20^{o}C) and with Sodium Dodecyl Sulfonate (SDS) and Oleic Acid (OA) as surfactants. Several concentrations in nanoparticles were considered, such as 0.01, 0.05 and 0.10 vol.% respectively. Also, the nanofluid properties were experimentally evaluated in the temperature range from 253.15 to 293.15K to verify the performance of such nanofluids in cold condition and demonstrate their potential as coolants.

2. Experimental Methods

2.1. Nanoparticles and Nanofluid Preparation

All the chemicals were purchased from Merck and used as received. Similarly to the reference [20], firstly, 2.0 grams of $FeCl_2.4H_2O$ and 8.13 grams of $Fe(NO_3)_3.9H_2O$ were dissolved in deionized water and the solution was ultrasonicated for 10 min. Then the solution was added dropwise to 300 ml of NH_4OH (33%) under ultrasonication at 70^{o}C. After 60 min, a brown powder at pH around 13.4 was collected by centrifugation, washed with deionized water several times until the pH of 7 was obtained, then dried at 80^{o}C and calcined at 400^{o}C for 2 hours. This procedure finally leads to the production of Fe_3O_4 nanoparticles according to equation 1.

$$FeCl_2 + 2Fe(NO_3)_3 + 8NH_4OH \rightarrow Fe_3O_4 + 2NH_4Cl + 6NH_4NO_3 + 4H_2O \quad \textit{Equation 1}$$

These nanoparticles were directly used for the preparation of nanofluids. A mixture of pure water and ethylene glycol with volume ratio of 50:50 at 293.15 K (W:EG 52.8:47.2 by weight) is used as a base fluid with the amount of 0.2 wt% in Sodium Dodecyl Sulfonate (SDS) and 0.2 vol% in Oleic Acid (OA) to disperse and stabilize Fe_3O_4 nanoparticles. A WEG-based Fe_3O_4 NFs with volume concentration of 0.1 vol% is prepared by dispersing a known weight of nanoparticles in the base fluid using ultrasonic mixing for 30 min. A probe sonicator (Qsonica, USA, LLC 60Hz, Q700W, Sonication Pulse Rate: 1 s ON, 1 s OFF, sonication power 80%) is used to disperse the nanoparticles into the fluid. A laboratory double-layer jacketed beaker is also used to control the sample temperature during the ultrasonic process. The NFs with 0.05 vol% and 0.01 vol% in NPs are similarly produced from the proper amount of nanoparticles and base fluid with the same amount of SDS and OA, meaning that the concentrations of surfactants were constants for all samples.

2.2. Characterization of Nanomaterials

The crystal structure of Fe_3O_4 nanoparticles was identified by X-ray diffraction (XRD) patterns using an X' Pert Pro diffractometer (Philips, PW 1800 X-ray, Netherlands) with Cu Ka (λ = 1.5406 Å) radiation in the angular domain of $10<2\theta<80$, respectively. The size and morphological characterization of the nanoparticles were examined by using a SEM (Philips, XL-30ESEM, Netherlands) with an operating voltage of 15 kV. Molecular sieve surface area and porosity of nanoparticles are obtained from N_2 adsorption measured at 77K on a BELSORP-mini II (BEL Japan Inc., Japan). Specific surface area was estimated by BET equation.

2.3. Rheological measurements

Rheological measurements of nanofluid and base fluid samples are carried out with a stress-controlled rheometer (Malvern Instruments Ltd, Malvern Kinexus Pro, UK) with a cone-plate geometry with a diameter of 60 mm, a cone angle of 1^o and a gap of 0.03 mm (**Error! Reference source not found.**). The temperature is controlled by a Peltier temperature control device placed below the lower plate to maintain the temperature with a precision of ±0.01 K. A thermal bath circulator with a mixture of water and EG as refrigerant fluid was used to achieve negative temperatures for rheological measurements.

Tests under steady-state condition and imposed shear stress are performed to cover a shear rate range from 10 to 1000 s^{-1} with at least 10 points per decade. To ensure a constant temperature within the sample gap, solvent trap covers were also used. Experiments were realized from 253.15 to 293.15K. Additional informations about this experimental instrument and the measuring operation can be found in Cabaleiro et al. [21]. First, the mixture of pure water and ethylene glycol with volume ratio of 50:50 was tested in the studied temperature range. As expected, a Newtonian behaviour was reported for this mixture in the shear rate range 10-1000 s^{-1} as shown later in Figure. The viscosity values of the mixture of pure water and ethylene glycol with volume ratio of 50:50 are reported in Figure 1 and were favourably compared to ASHRAE data with an *AAD* (Absolute average deviation) less than 3 % in the tested temperature range [22].

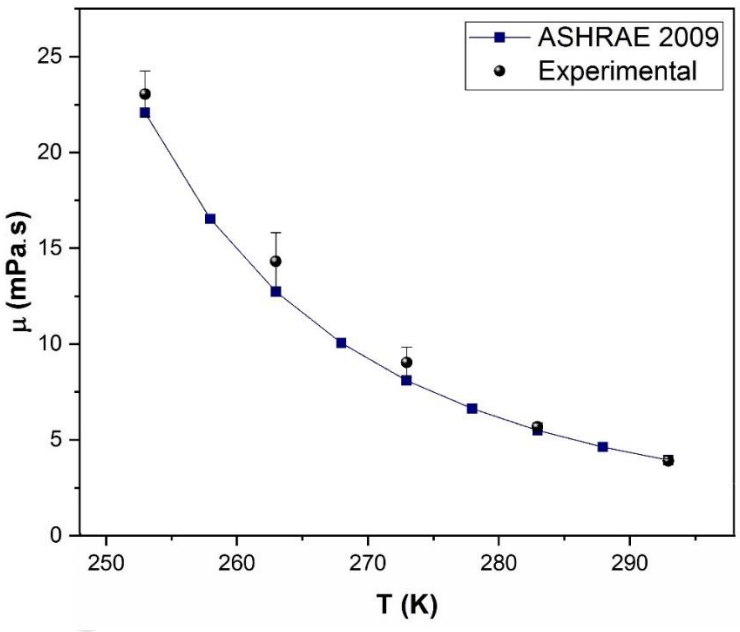

Figure 1. Comparison of experimental and ASHRAE viscosity values [22] of ethylene glycol and water mixture (50:50 vol.vol)

2.4. Thermal conductivity measurements

A THW-L2 Portable thermal conductivity meter (Thermtest Inc., Canada) based on the transient short hot-wire (THW) technique following the ASTM D7896 standard was used to measure the thermal conductivities of base fluid and nanofluids from 263.15 to 293.15K. The THW-L2 can be used to measure thermal conductivity of liquids from 0.01 to 2 W/mK and between 263.15 and 373.15K, and a small volume of 20ml is only required. The wire is

made of alumel with a length of 60 mm and a diameter of about 0.1 mm. In the experimental procedure, the container is first filled with the tested sample. Then, the probe is introduced within the sample. Finally, the container is placed within a dry bath. Once the required temperature sample is achieved and stabilized the thermal conductivity measurements starts. A test time of 2s was considered to avoid convective effects. For each sample, the THW sensor wire is heated by using a regular power supply of about 90 mW that leads to a temperature rise between 1.1 and 1.4 for all samples. The temperature rise is recorded by monitoring the wire's change in electrical resistance. The thermal conductivity is classically determined by the slope of the temperature rise plot versus the time logarithm in the linear region from the THW-L2 software. It should be mentioned that both the probe temperature sensor and hot wire sensor have been carefully calibrated with distilled water at 273.15K. The calibration was regularly checked with no significant deviation after nanofluid measurement. Finally, the probe and the container were also carefully cleaned and washed with acetone and distilled water respectively between each tested sample. Five values of thermal conductivity measurements are taken for each sample and each temperature with 5 mins between measurements. In the following, the thermal conductivity values are an average of these measurements, the error bars corresponding to the standard deviation. As for viscosity, the thermal conductivity of the mixture of pure water and ethylene glycol with volume ratio of 50:50 was compared to ASHRAE data. An AAD (Absolute average deviation) less than 1.5 % was obtained in the temperature range 263.15/293.15K [22].

2.5. Surface Tension (ST) measurements

The surface tension between the surrounding area and both the base fluid and nanofluids was evaluated by Drop Shape Analyzer DSA30 (KRÜSS GmbH, Hamburg, Germany) on the basis of the pendant drop technique in the 253.15 to 293.15K temperature range. DSA30 was supplied with a syringe system, a standardized LED lighting unit, high-quality optical components, and a high-resolution camera. A temperature control chamber, a module for controlling humidity, and a circulator bath were used in order to achieve stable internal temperature and humidity. To avoid condensation and icing of the viewing windows, a gas flow system can also be connected.

The shape of sample drops formed at the end of a vertical syringe was recorded and analyzed when the drop suspended from the needle's apex. The surface tension is evaluated from the drop shape analysis through balancing internal and external forces acting on the drop by the Young-Laplace equation. The increase in pressure inside the droplet is due to the interfacial tension between the internal and external phases. A needle with an outer diameter of 1,835 mm was used to produce drops under well-controlled flow rate. Additionally, the assessment of the drop shape was repeated without any significant deviations between measurements. The uncertainty of surface tension measurements with this device was estimated to be less than 1% in previous studies [21, 23].

3. Results and Discussion

3.1. Characterization of nanoparticles

The XRD patterns of the crystalline Fe_3O_4 are shown in Figure 2. Diffraction peaks of the Fe_3O_4 (JCPDS file No. 75-0449) are indicated at 30.3°, 35.7°, 43.3°, 53.7°, 57.3° and 62.9°, and correspond to the crystallographic planes of (220), (311), (400), (422), (511), and (440), respectively. Although the patterns Fe_3O_4 and α-Fe_2O_3 phases are similar, no trace of the peaks corresponding to α-Fe_2O_3 can be seen [16, 24]. An average crystal size of 10 nm is obtained from the Scherrer equation, defined by $D=0.9\lambda/(\beta\cos\theta)$. In this well-known equation, D is the diameter of the nanoparticles, θ is the diffraction angle of the peak of the cubic phase, λ is the X-ray wavelength (Cu Kα =0.15406 nm in the angular domain of $10<2\theta<80$) and β is the full width at half maximum (FWHM) of the sharp and strong peak in radian [20].

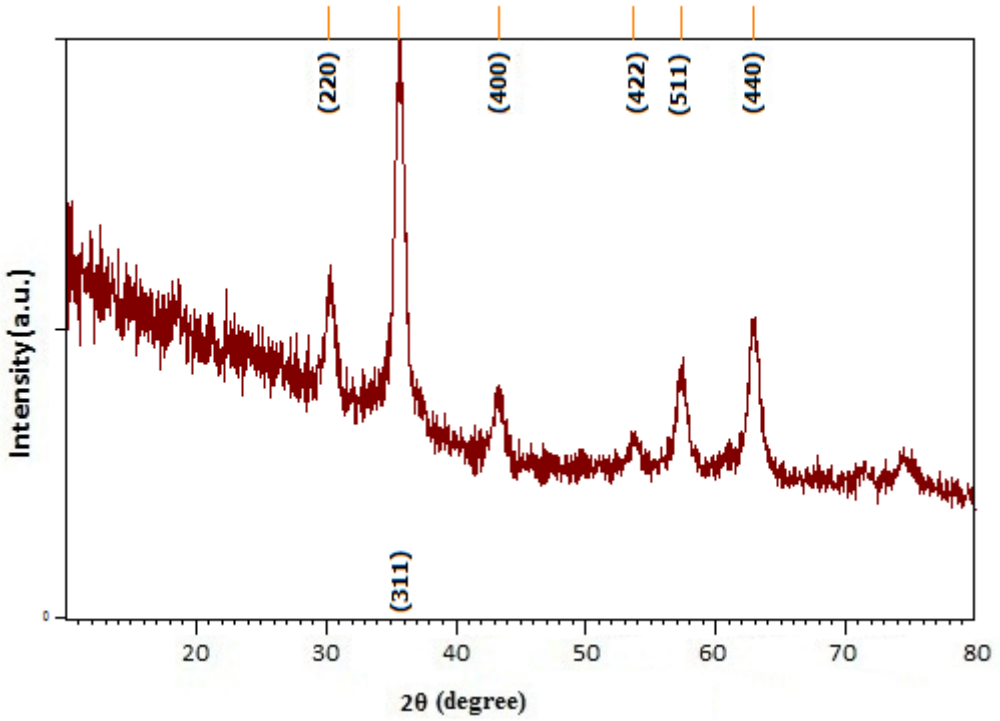

Figure 2. XRD of Fe_3O_4 synthesized by precipitation method

The morphology of the magnetic Fe_3O_4 nanoparticles was investigated by SEM. Figure 3 shows that nanoparticles are mainly spherical in shape with a size of about 20-60 nm, and in powder form they tend to form aggregates.

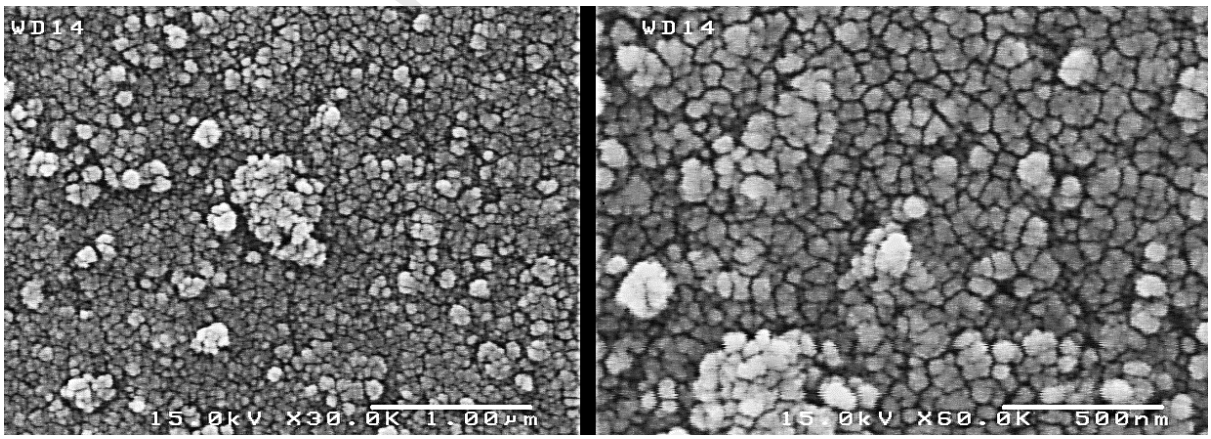

Figure 3. SEM images of Fe_3O_4 nanoparticles

The type IV of N_2 adsorption-desorption isotherm and pore size distribution of Fe_3O_4 nanoparticles are described in Figure 4. The BET surface area, pore volume, and the average pore size of Fe_3O_4 are determined to be about 114 m^2/g, 0.77 cm^3/g, and 22.1 nm,

respectively. The average spherical-shape approximated sizes of the nanoparticles from BET specific surface equation was calculated as $d_{BET} = 6000/(\rho \times S_{BET})$, where S_{BET} is surface area (m^2/g) and ρ is the skeletal density (g/cm^3) [24]. An average size of 10.1 nm is found that is in agreement with the crystallite size calculated by XRD Scherrer equation.

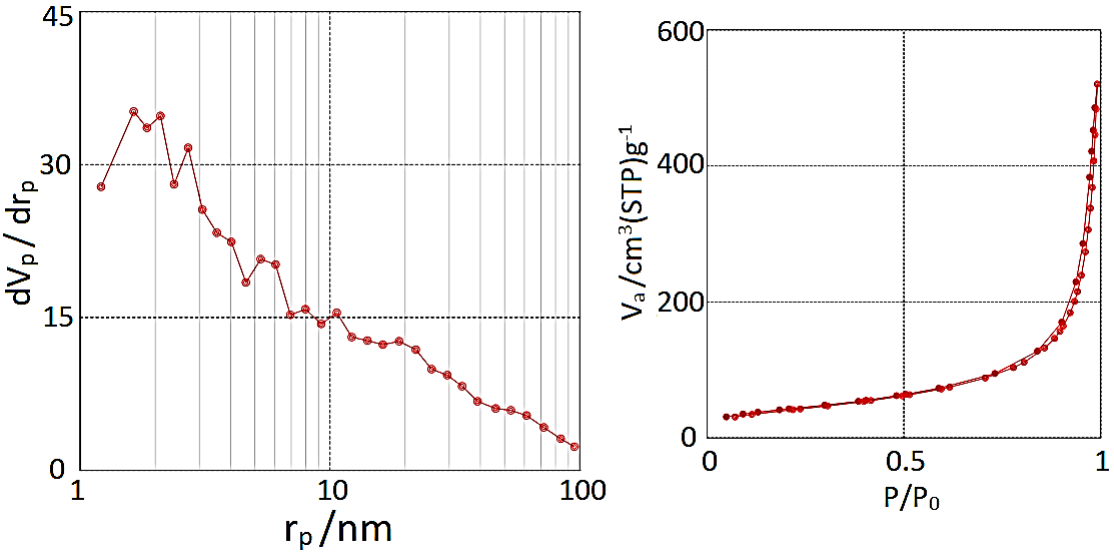

Figure 4. N_2 adsorption/desorption isotherms and pore diameter distribution of Fe_3O_4

3.2. Shear flow behaviour and viscosity of nanofluids

Newtonian or non-Newtonian behaviour of nanofluids can be evaluated from steady-state shear flow curves that relate shear stress or apparent viscosity to shear rate. By definition, when shear stress shows linear relationships with shear rate and the apparent viscosity remains constant with shear rate, the behaviour is Newtonian [15]. It is defined by the following relationship (Eq2).

$$\tau = \mu\dot{\gamma} \qquad \textit{Equation 2}$$

where μ is the apparent viscosity, τ is the shear stress, and $\dot{\gamma}$ is the shear rate.

When shear stress follows a power law with shear rate, a non-Newtonian behaviour is obtained, as shown by the following equation.

$$\tau = \mu\dot{\gamma}^n \qquad \textit{Equation 3}$$

With n the flow index. When n<1, a shear-thinning behaviour is defined – in that case apparent viscosity decreases with shear rate - while shear-thickening corresponds to n>1.

First, the shear flow curves of ethylene glycol-water mixture (WEG) with the presence of surfactant and the effect of temperature are reported in Figure 5. This figure shows that the presence of surfactant do not significantly affect the behaviour of ethylene glycol-water mixture in the temperature range 273.15-293.15K. Actually, a Newtonian behaviour is noticed without significant change in viscosity value. However, a non-Newtonian behavior is found for WEG with surfactants at sub-zero temperature especially at 253.15K and with less effect at 263.15K. At these temperatures, the shear flow curves indicate that the viscosity values reduce when the shear rate increases leading to a shear-thinning behaviour. A similar phenomena was previously reported by Kiani et al. [25]. Such a behaviour can be attributed to oleic acid as explained in the following.

Oleic acid is easily or reasonably miscible in ethylene glycol and partially soluble in water. Also, this soluble carboxylic acid dissociates hydrogen ions to an extent in water. Viscosity, melting point, and solidification to crystalline mass (freezing point) of oleic acid are 38.80 mPa.s (@293.15K), 286.15K, and 277.15K respectively [26]. Also, Salih et al. [27] reported a cloud point (CP) and a pour point (PP) of about 283.15K±1 and 273.15K±1 for oleic acid, respectively. The cloud point is the temperature at which the fluid starts to cloud as a result of crystallization under coordinated cooling, such as wax. Under this condition, the surfactant is no longer fully soluble, but rather precipitates as a second phase providing the fluid a cloudy texture. The cloud points is distinct property for non-ionic surfactants. The pour point of a liquid is the temperature in which the change in flow properties occurs [28]. At cold operating temperatures, surfactants also gather together and form an emulsion in the mixture like waxes in the petroleum industry [29].

Consequently, the cloud point demonstrates the tendency of surfactant to exist as solid particles in a liquid. Thus, the pour point and cloud point are substantial indexes of the low-temperature fluidity of oleic acid. This surfactant tends to create macro crystalline structures at colder temperatures. Such macro-crystals limit the system's simple flow owing to the respective molecules' reduction of kinetic energy during self-aggregation and provide greater resistance in static state as well as at lower shear rates that can explain the increase

of viscosity. Higher the content in oleic acid, higher is the crystallization effect leading to the shear-thinning enhancement and the viscosity increase.

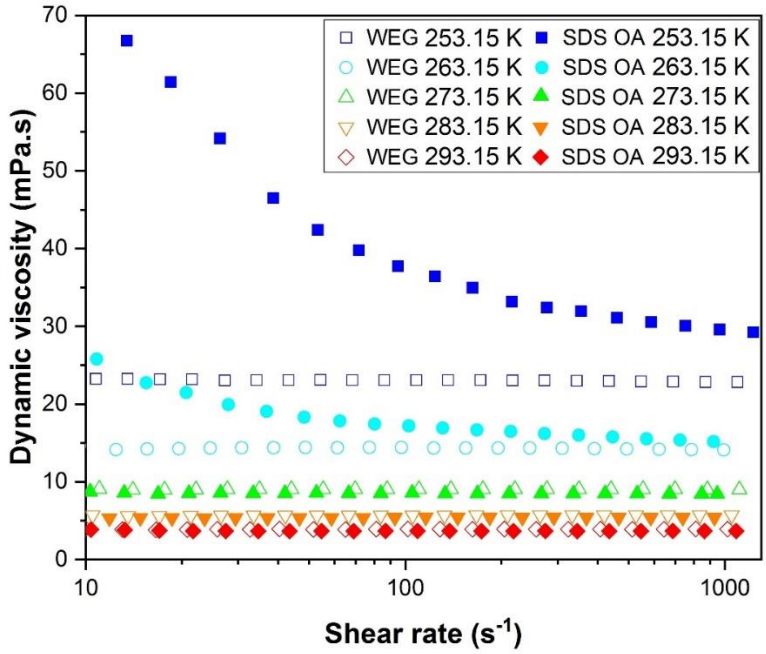

Figure 5. Shear flow curves for the mixture Water and Ethylene Glycol – Impact of surfactant and temperatures

The shear flow curves of Fe_3O_4 nanofluids with volume concentration range of 0.01%–0.1% and in the temperature range of 253.15K – 293.15K are described in Figure 6. It is observed from this Figure that nanofluids behave in a Newtonian manner for temperature range 263.15K – 293.15K as the viscosity is independent of the shear rate. A similar trend was noticed by Sundar et al. [16] with Fe_3O_4 nanoparticles suspended in different WEG mixture (40:60 , 60:40, and 80:20 percent by weight respectively) in temperature range 273.15-323.15K. As well, Namburu et al. [11] reported also a Newtonian behaviour for nanofluids made of CuO nanoparticles in 40:60% WEG mixture in the temperature range 238.15 - 323.15K. Instead, at 253.15K, the viscosity of nanofluids decreases with shear rate, indicating a shear-thinning behaviour. More surprisingly is the effect of nanoparticle concentration increase, in particular at negative temperature that leads to the reduction of nanofluid viscosity. To evidence such an effect, the nanofluid viscosity at high shear rate is reported in Figure 7for all concentrations and temperatures. For non-Newtonian nanofluids, an average of viscosity values in the shear rate range of 700-1000s^{-1} was considered.

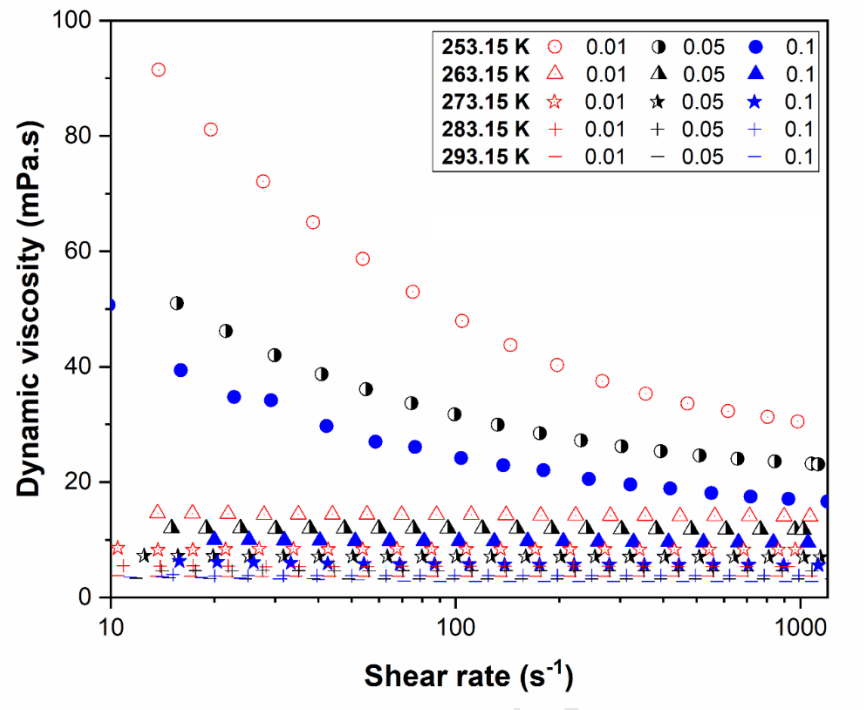

Figure 6. Apparent viscosity versus shear rate of nanofluids with various nanoparticle volume concentrations in function of temperature.

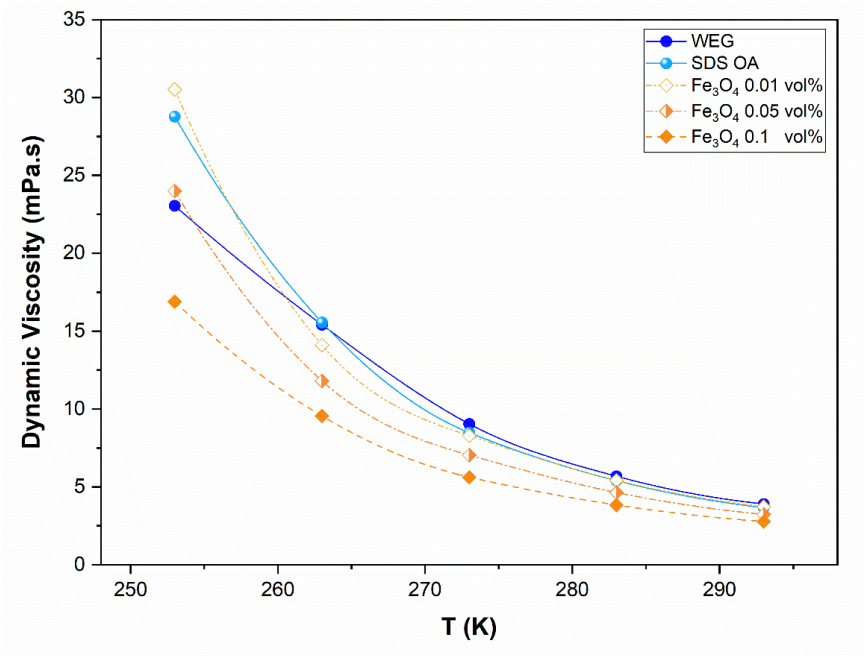

Figure 7. Experimental values of viscosity for various volume concentrations of nanofluids with respect to temperature.

Such a non-Newtonian behaviour observed at 253.15K and the reduction of viscosity with nanoparticle content is linked to the nanoparticles adsorption of the molecules of oleic acid

at their surfaces that reduces, at low temperature, the amount of oleic acid solidified in the liquid mixture and therefore the induced thinning.

As shown in the Figure 7, the nanofluid viscosity decreases with temperature increase as mentioned in most of literature reports [11, 15, 31, 32]. Figure 8shows lower viscosities and independency of temperature with respect to both the base fluid and the base fluid with surfactant at higher nanofluid concentrations. This also demonstrates the consistency of the experimental results trend. It should be emphasized also that dependency of viscosity on nanoparticle concentration is far from intuitive [33]. Some authors [34, 35] indicate a lubricating effect for some mixtures leading to a reduction in viscosity. This lubricating effect was reported to be dependent on nanoparticles content and more pronounced at small concentrations. Yang et al. [30] argued that the adsorbed layer is created in the presence of oleic acid in the base fluid so that the steric repulsion controls the particle interaction and led to reduce the viscosity. Therefore, oleic acid can be considered as a booster to decrease the effective viscosity at low concentration of nanoparticles.

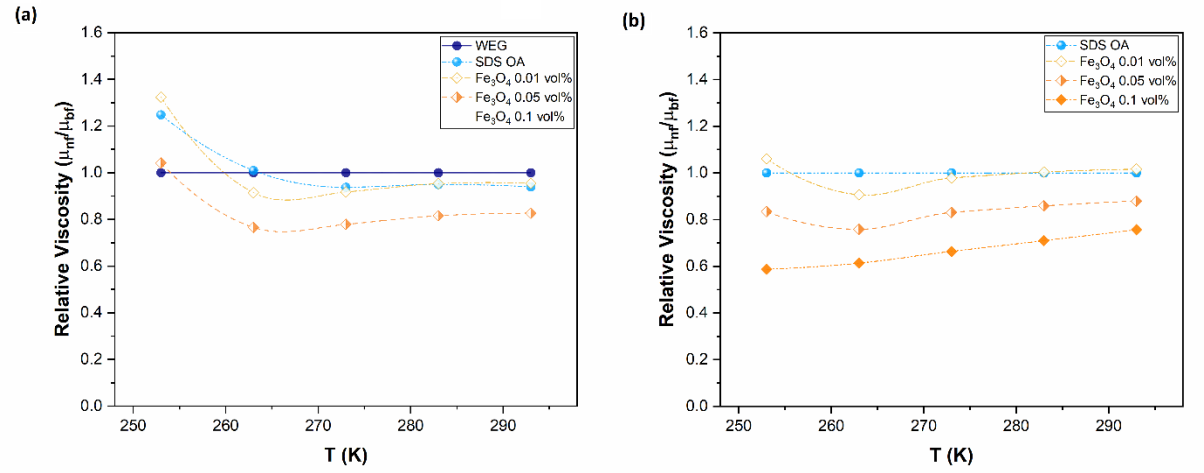

Figure 8. Relative viscosity and temperature relationship for various concentrations of Fe_3O_4 a) compared to base fluid properties without surfactant, b) compared to the actual base fluid (with surfactant).

For temperature dependence modelling, a well-developed generalized fluid viscosity correlation proposed by Kurkarni et al. [11, 32] described by the following equation was used.

$$ln\,\mu_{nf} = A\left(\frac{1}{T}\right) - B \qquad \textit{Equation 4}$$

where μ_{nf} is the nanofluid viscosity in mPa·s, T is the temperature in Kelvin, and A and B are polynomials depending on nanoparticle volume concentration, defined later in equation 6.

Here, A and B are here expressed as follows:

$$A = -30645\ (\emptyset)^2 - 1858(\emptyset) + 3863.8 \quad with\ R^2 = 0.99$$

$$B = 103.96(\emptyset)^2 - 3.4445(\emptyset) + 18.835 \quad with\ R^2 = 0.99$$

3.3. Thermal conductivity of nanofluids

The thermal conductivity measurements and the thermal conductivity ratio of Fe_3O_4 WEG-based nanofluids are shown in Figure 9in function of temperature and volume concentrations. First, it is shown that the presence of surfactant within the WEG mixture does not significantly affect the thermal conductivity, even at 263.15K, where surfactant crystal could be present. Then, the figures clearly evidence the effect of both the nanoparticle content and temperature on the thermal conductivity enhancement of nanofluids. It can be seen that even at the low concentration range studied here (<0.1%), the thermal conductivity is significantly enhanced by nanoparticles. This enhancement increases with the volume fraction of the nanoparticles. The ratios of the thermal conductivity are increased by nearly 14.3%, 9.5% at highest and lowest operating temperature at the highest volume fraction, 0.1 vol%. Likewise, Sundar et al. [16] reported that the thermal conductivity of magnetic Fe_3O_4 water-ethylene glycol nanofluid including CTAB as surfactant is improved with temperature.

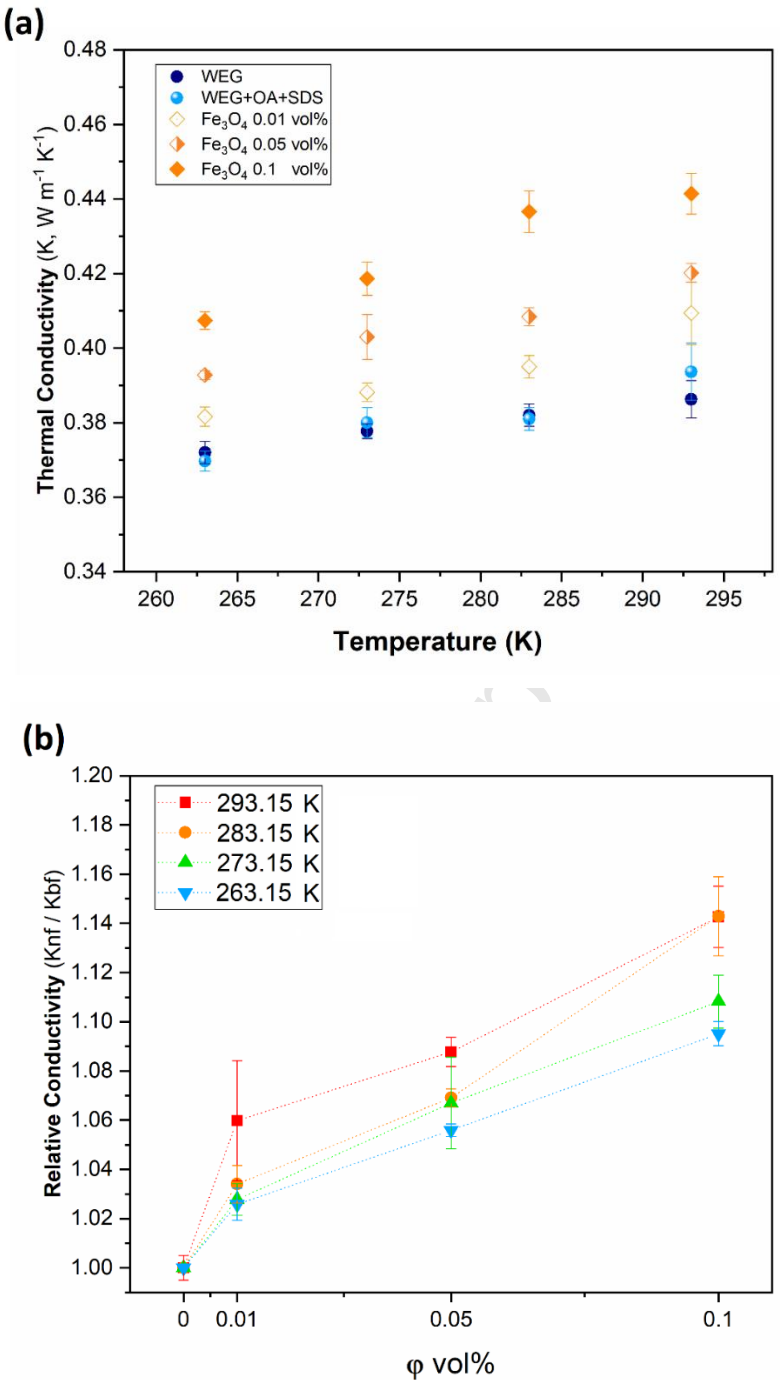

Figure 9. Thermal conductivity (a) and relative thermal conductivity (b) of nanofluids as a function of temperature and volume concentration.

In an attempt to understand the phenomena that could be responsible of such thermal conductivity enhancement, some models from the literature are considered in the following [36-42]. Many complex and possibly coupled mechanisms shown in Figure 10have been considered in the past to use or develop theoretical models for thermal conductivity of nanofluids such as classical effective theory, nanoscale layer, agglomeration and

aggregation, Brownian motion, etc [38, 43]. These models are here presented then compared to experimental data.

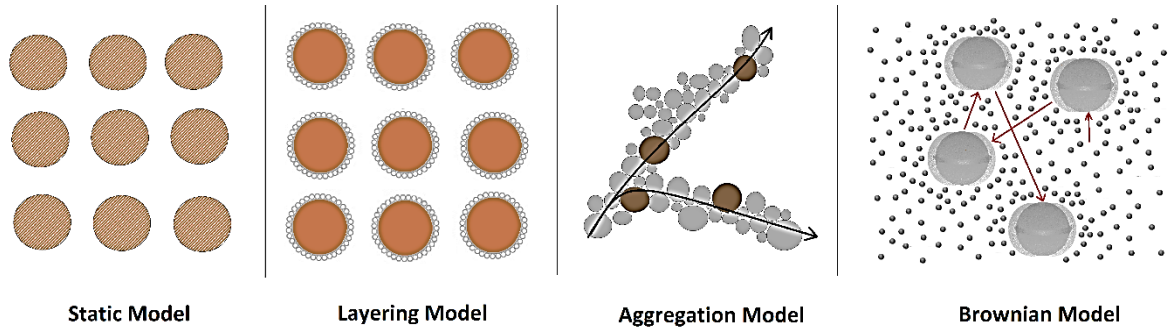

Figure 10. Various mechanisms for thermal conductivity models such as classical Maxwell theory, the formation of an orderly liquid layer around nanoparticles, aggregation, and Brownian motion.

As a static model, the Maxwell equation is obtained by solving Laplace's equation considering a diluted suspension of spherical particles and neglecting their interactions. The equation writes [38]:

$$\boldsymbol{k_{nf}} = \frac{\boldsymbol{k_p}+2\boldsymbol{k_{bf}}+2(\boldsymbol{k_p}-\boldsymbol{k_{bf}})\boldsymbol{\phi}}{\boldsymbol{k_p}+2\boldsymbol{k_{bf}}-(\boldsymbol{k_p}-\boldsymbol{k_{bf}})\boldsymbol{\phi}}\boldsymbol{k_{bf}} \qquad \textit{Equation 5}$$

Where k_{bf}, k_p, and k_{nf} are the thermal conductivity of the base liquid, nanoparticles (np), and the nanofluid, respectively, and ϕ is the volume fraction of the particles. The volume fraction is calculated from the following Equation in percentage:

$$\phi = \frac{\frac{W_{np}}{\rho_{np}}}{(\frac{W_{np}}{\rho_{np}}+\frac{W_{bf}}{\rho_{bf}})} \times 100 \qquad \textit{Equation 6}$$

where, ρ_{np}, the density of Fe_3O_4 nanoparticles, is 5180 kg/m^3 [44], the density of WEG (ρ_{bf}) as the base fluid is taken from ASHREA data [22]. W_{np} and W_{bf} are the weight of nanoparticles and the base fluid, respectively. k_{bf}, the thermal conductivity of the base liquid, is taken from experimental data at different temperatures. The average value of 0.3863, 0.382, 0.3777, 0.372 Wm^{-1}K^{-1} are corresponding for 293.15, 283.15, 273.15 and 263.15K, respectively (see Figure a). The thermal conductivity of Fe_3O_4 nanoparticles is considered as 17.7 Wm^{-1}K^{-1} according to the literature [45].

The Yu and Choi [46] model derives from the Maxwell model by considering the effects of the nanolayer and assuming that there was no particle interaction at lower nanoparticle

fractions. It expresses as follows:

$$\boldsymbol{k_{nf}} = \frac{\boldsymbol{k_p+2k_{bf}+2(k_p-k_{bf})(1+\beta)^3\phi}}{\boldsymbol{k_p+2k_{bf}-(k_p-k_{bf})(1+\beta)^3\phi}}\boldsymbol{k_{bf}} \qquad \textit{Equation 7}$$

β is the ratio of the nanolayer thickness to the original particle radius and β= 0.1 was usually assumed to evaluate the nanofluid effective thermal conductivity. This model can predict potentially the effect of nanolayers when the particle diameter would be less than 10nm [46].

Prasher et al. [47] proposed a model taking into account the impact of aggregation on the effective thermal conductivity that was later modified by Evans et al. [48] to include the cluster size effect. According to SEM results, the dead ends particles with nanolayer are considered, therefore, the effective thermal conductivity is then given by:

$$\boldsymbol{k_a} = \boldsymbol{(1-\phi_{int})k_{nl}+\phi_{int}k_p} \qquad \textit{Equation 8}$$

$$\boldsymbol{k_{nf}} = \frac{\boldsymbol{k_a+2k_{nl}+2(k_a-k_{nl})\phi_a}}{\boldsymbol{k_a+2k_{nl}-(k_a-k_{nl})\phi_a}}\boldsymbol{k_{nl}} \qquad \textit{Equation 9}$$

In these equations, $\mathrm{k_{nl}}$ is the thermal conductivity of particles with nanolayer. The volume fraction of nanoparticles in the aggregate is denoted ϕ_{int} and the volume fraction of aggregate in the fluid ϕ_{a} are obtained respectively by the followings equations $\phi_{\mathrm{int}} = (\mathrm{d_a}/\mathrm{d_p}(1+\beta))^{\mathrm{d_f}-3}$ and $\phi_{\mathrm{nl}} = \phi_{\mathrm{int}}\phi_{\mathrm{a}}$. Here, the diameter of aggregate $\mathrm{d_a}$ is assumed as 40nm (average diameter of SEM results), the nanoparticle size $\mathrm{d_p}$ is considered as 10 nm (from XRD results) and the value of 2.5 is considered for $\mathrm{d_f}$ [48], due spherical shape of nanoparticles, and the volume fraction of nanoparticle combined with nanolayer is calculated by $\phi_{\mathrm{nl}} = (1+\beta)^3\phi$.

Prasher et al. [49] suggested a model considering the nanoparticle's random motion-induced fluctuation to predict thermal conductivity of nanofluid. They have demonstrated that the nanoconvection caused by Brownian motion is a strong mechanism for analyzing the nanofluid thermal conductivity enhancement. This model is defined as follows:

$$\boldsymbol{k_{nf}} = \boldsymbol{(1+ARe^m Pr^{0.333}\phi)}\left(\frac{\boldsymbol{k_p(1+2\alpha)+2k_{bf}+2(k_p(1-\alpha)-k_{bf})\phi}}{\boldsymbol{k_p(1+2\alpha)+2k_{bf}-(k_p(1-\alpha)-k_{bf})\phi}}\right)\boldsymbol{k_{bf}} \textit{ with } Re = \frac{1}{\vartheta}\sqrt{\frac{18k_bT}{\pi\rho_p d_p}}$$

Equation 10

In this equation, α is the nanoparticle Biot number defined as $\alpha = 2R_b k_{bf}/d_p$. A constant value for R_b of 0.77×10^{-8} and 1.2×10^{-8} m^2K/W are assumed for water-based and EG-based nanofluids respectively. The amount of 4×10^4 and 2.05 (average of m=2.5 for water and m=1.6 for EG) are considered for A and m as a first guess, respectively [41, 49]. Actually, A and m were determined by experiments and m=1.33 is considered to achieve a good agreement in the results. For this model, the particle sizes from XRD results were used as d_p=10 nm.

Pang et al. [50] suggested a comprehensive model for thermal conductivity of nanofluids with combination of classical effective theory, nanolayer, aggregation and nano-convection effect. This model writes as follows:

$$\boldsymbol{k_{nf}} = [\mathbf{1} + \frac{\boldsymbol{\phi_a}(\boldsymbol{k_a}-\boldsymbol{k_{bf}})}{(\mathbf{1}-\boldsymbol{\phi_a})/\boldsymbol{n}(\boldsymbol{k_a}-\boldsymbol{k_{bf}})+\boldsymbol{k_{bf}}} + (\boldsymbol{A_1}\, \boldsymbol{ln}(\boldsymbol{A_2}\boldsymbol{\phi_a}\boldsymbol{Re_a}^{\boldsymbol{m}}\boldsymbol{Pr}^{\mathbf{0.333}}) + \boldsymbol{A_3})(\frac{\mathbf{1}+\mathbf{2}\boldsymbol{\phi_a}+\mathbf{2}(\mathbf{1}-\boldsymbol{\phi_a})\,\boldsymbol{\alpha}}{\mathbf{1}-\boldsymbol{\phi_a}+(\mathbf{2}+\boldsymbol{\phi_a})\,\boldsymbol{\alpha}})]\boldsymbol{k_{bf}}$$

$$\textit{with } Re_a = \frac{1}{\vartheta}\sqrt{\frac{18k_bT}{(n-2)\pi\rho_a d_a}} \qquad \textit{Equation 11}$$

where A_2 corresponds to A in equation 10. Similar values than in equation 10 were considered for A and m. n equals 3 for spherical nanoparticles. A_1 and A_3 are adjusting parameters. The density of aggregate ρ_a is calculated by $\rho_a = (1-\phi_{int})\rho_{bf} + \phi_{int}\rho_{int}$ where $\rho_{int} = \rho_{bf} + \frac{\rho_p-\rho_{bf}}{(1+\beta)^3}$.

The comparison of thermal conductivity of nanofluids from experimental results and theoretical models previously described are shown in Figure 11. As traditional models, the Maxwell and Yu models are weak to predict thermal conductivity at low concentrations. However, the dynamic model suggested by Prasher et al. [46] can partially (at m = 1.33) describe the behaviour of temperature-dependent thermal conductivity of nanofluids, in particular for temperatures higher than 273.15K as indicated in Figure but it is not consistent with the nonlinear evolution of experimental data at low nanoparticle content and for negative temperatures. Finally, it is shown that the model of Pang et al. [50] is in good agreement with the experimental data for all temperatures and concentrations (see Figure 11). The Pang et al. model, an aggregation based model for thermal conductivity enhancement of nanofluids, includes the classical effective medium theory, the nanolayer effect of molecules around the solid particle, Brownian motion of nanoparticles

encompassing aggregation and nano-convection [50]. This evidences that the thermal conductivity enhancement is linked to several coupled physical phenomena.

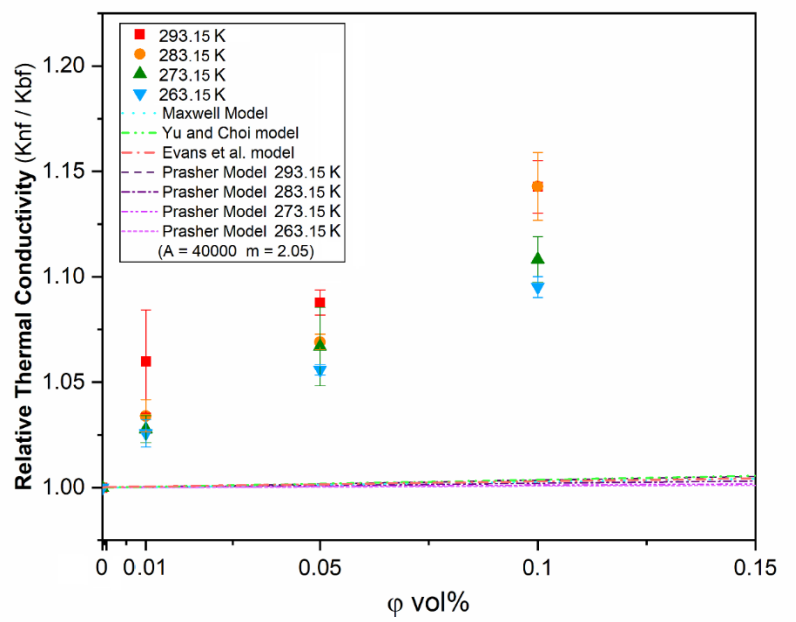

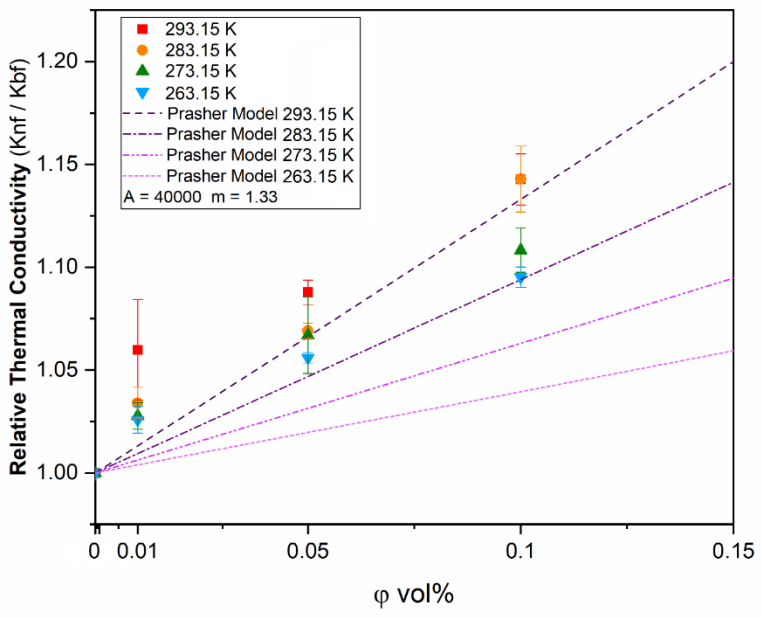

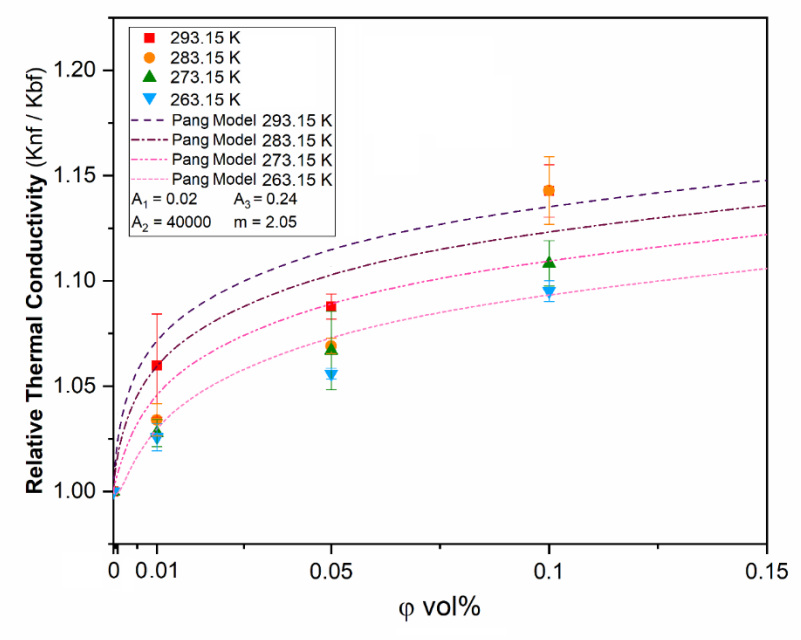

Figure 11. Comparison of thermal conductivity improvement vs theoretical models.

3.4. Surface Tension results

Surface tension (ST) is a very significant parameter in heat transfer phenomena of boiling, condensation, and two-phase flow [51]. This literature review, [51], evidences that the surface tension of nanofluids is usually reduced by increasing temperature. It is also reported that changes in surface tension due to the dispersion of nanoparticles, can raise, reduce or not be affected with nanoparticles loading based on the nature and size of nanoparticles and base fluid and their interaction as recently illustrated in [52, 53, 54, 55].

First, nanofluid densities required for surface tension analysis were evaluated by the following theoretical correlation, see Equation 12. All the data are gathered in Table 1.

$$\rho_{nf} = \left(V_p \rho_{bf+\,surfactants}\right)\phi\ \rho_{np} + (1-\phi)\rho_{bf\,+\,surfactants} \qquad \textit{Equation 12}$$

where, ρ_{nf} is the density of nanofluid, ρ_{np} is the density of nanoparticles that is assumed to be not strongly modified with temperature and is considered about 5180 kg/m^3 [44], and $\rho_{bf+surfactants}$ is the density of the base fluid with surfactants. The density of SDS and OA are 1010 and 895 kg/m^3, respectively, at 298.15K [56]. V_p, that is the pore volume, is taken as 0.77 cm^3/g based on the BET result reported earlier. Accordingly, densities of surfactants are close to density of WEG and their content is low, therefore, it is assumed that the density of

WEG with surfactants was not significantly changed. The density of WEG at the studied temperatures was taken from ASHREA data [22].

Table 1.Theoretical density and experimental surface tension (ST) values for the nanofluids.

Fluids	WEG		WEG SDS OA		Fe_3O_4 0.01 vol%		Fe_3O_4 0.05 vol%		Fe_3O_4 0.1 vol%	
T (K)	ρ ($Kg.m^{-3}$)	ST (mN/m)	ρ ($Kg.m^{-3}$)	ST (mN/m)	ρ ($Kg.m^{-3}$)	ST (mN/m)	ρ ($Kg.m^{-3}$)	ST (mN/m)	ρ ($Kg.m^{-3}$)	ST (mN/m)
253.15	1.087	61.34±0.28	1.087	33.91±1.00	1.087	34.45±0.73	1.089	35.71±1.05	1.091	46.88±0.41
263.15	1.084	60.96±0.25	1.084	31.98±0.44	1.084	32.09±0.66	1.086	32.78±1.41	1.088	43.74±0.38
273.15	1.081	60.44±0.18	1.081	30.75±0.68	1.081	31.27±0.64	1.083	32.31±1.25	1.085	41.09±1.01
283.15	1.078	59.41±0.11	1.078	30.26±0.73	1.078	30.71±0.98	1.080	32.23±1.12	1.082	39.81±1.41
293.15	1.074	58.87±0.21	1.074	30.17±0.75	1.074	30.57±0.68	1.076	31.91±0.84	1.078	40.05±1.22

Figure 12 shows the results of nanofluids surface tension obtained by the pendant drop method. This figure shows that surface tension values first decreases with time before to reach a quite stable and equilibrium value, except for WEG alone for which surface tension value is stable with time. Such a variation with time is known as dynamic surface tension [58]. The dynamic character of the surface tension during the process is triggered by the diffusion of surfactants on the solid surface of the needle used for producing drop that induces some changes in the wetting properties of the needle solid surface. In the following discussion, the surface tension values considered are the one obtained at the equilibrium and they are presented in Figure 13.

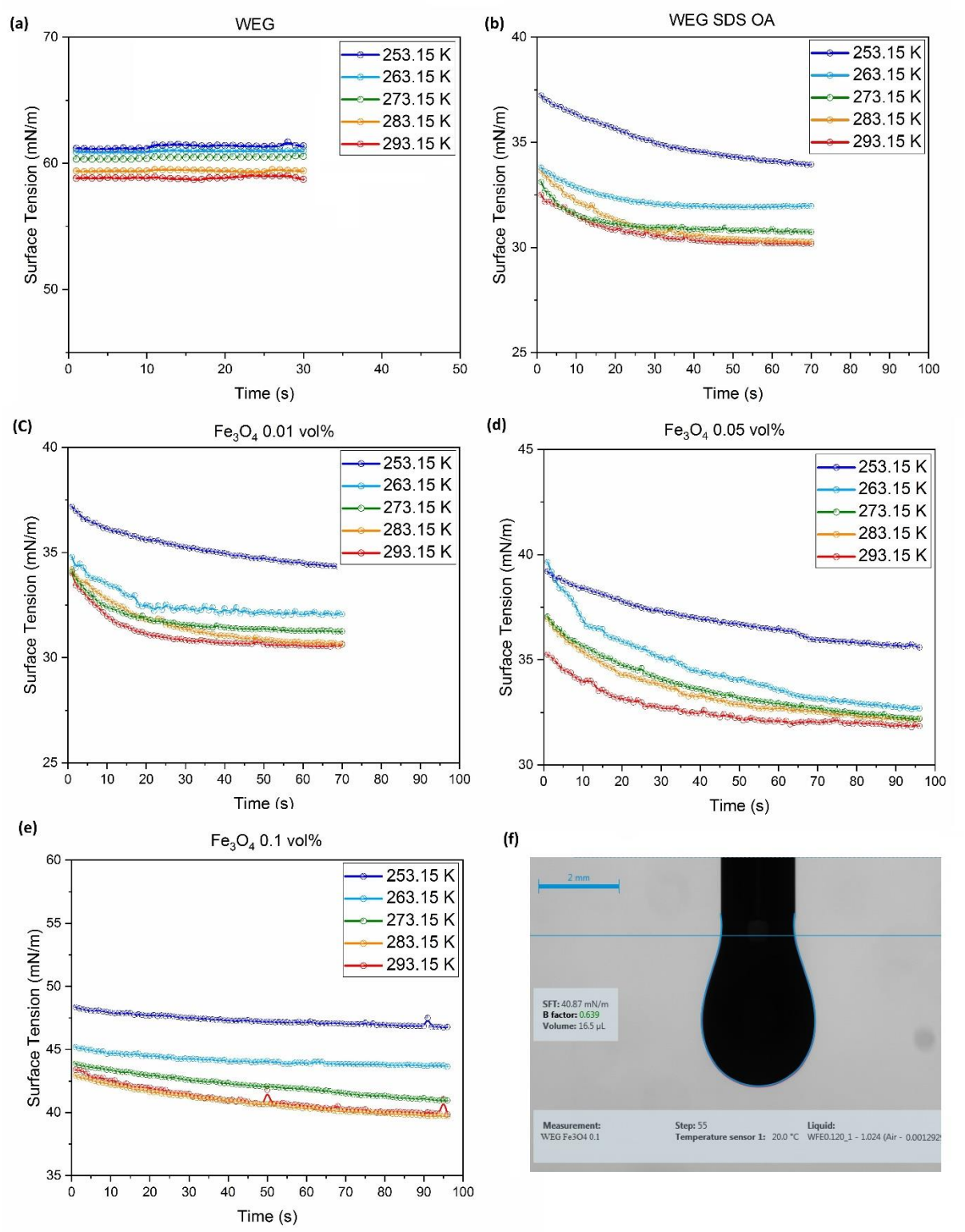

Figure 12. Dynamic surface tension of (a) water-ethylene glycol mixture (WEG 50:50) as the based fluid (b) the base fluid with surfactants Sodium Dodecyl Sulfonate (SDS, 0.2 wt%), and Oleic Acid (OA, 0.2 vol% (c) 0.1 (d) 0.05 (e) 0.1 volume percentage of Fe_3O_4 nanofluids, and (f) Pendant drop images of Fe_3O_4 nanofluids.

First, at expected for fluids, it is noted in Figures 12 and 13, as in Table 1, that surface tension of WEG and nanofluids decreases with temperature increase. Then, it is observed that with the presence of surfactant, the surface tension of WEG mixture is significantly decreased, suggesting that the base fluid surface tension is primarily controlled by surfactant. Actually, in that case, the surfactant molecules that are governed by Gibbs absorption phenomena try to form monolayer at the interface that results in the reduction of surface tension. This agrees with the results of Cheng et al. [58] and Radiom et al. [59] who studied the influence of SDS and OA to stabilize CNT and TiO_2 nanoparticles in water, respectively. They indicated the reduction in surface tension with the presence of surfactants. A reduction of about nearly 50% is here obtained for all temperatures. In the same Figures, one can see that surface tension of nanofluids increases as Fe_3O_4 loading increases, with almost 38%, and 33% at the highest concentration, 0.1% at 253.15K and 293.15K, respectively. Surfactant molecules are mainly adsorbed to most of the nanoparticles and not at the interface, this increases the surface tension. Finally, it should be mentioned that for the higher concentration in nanoparticles e.g. for the sample with the higher content in surfactant, the change in surface tension with temperature is more pronounced, and the increase in surface tension at sub-zero temperatures is more important. This can be related to the crystallization and the solidification of surfactant that reduces amount of available surfactant in solution for the nanoparticles and increase particles in the fluid.

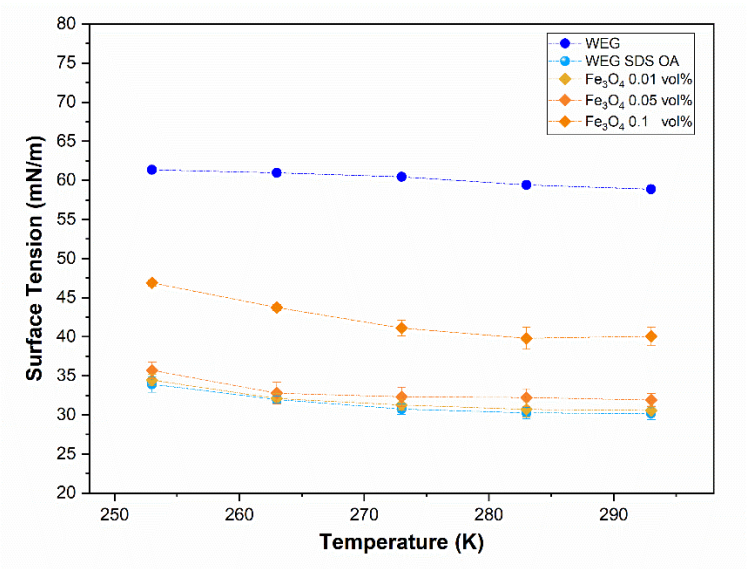

Figure 13. Surface tension values of nanofluids as a function of temperature and volume concentration.

4. Conclusion

The synthesis and the thermophysical characterization of Fe_3O_4 nanofluids were performed in this study. The nanofluids were produced with a mixture of deionized water (W) 50% and ethylene glycol (EG) (WEG 50%) and both sodium dodecyl sulfonate and oleic acid as surfactants. The thermal conductivity, dynamic viscosity and surface tension of these Fe_3O_4 nanofluids were measured for temperatures ranging from 253.15 to 293.15K and different volume concentrations of nanoparticles, 0.01, 0.05 and 0.1% respectively. It is shown that the thermal conductivity of nanofluids is dependant to nanoparticle concentration and temperature, while a comparison with some relevant theoretical models evidences the coupled effects of effective medium theory, nanolayer interface, Brownian motion of nanoparticles encompassing aggregation and nano-convection to explainthe thermal conductivity enhancement of nanofluids. Flow properties of nanofluids depend also on nanoparticle content and temperature. Remarkably, it was found that the dynamic viscosity of nanofluids decrease with nanoparticle content with a strong effect at 253.15K. The surface tension of nanofluids is also monitored by the content of nanoparticles. While the surface tension of WEG is first decreased by the presence of surfactants, it was shown that surface tension is then increased with Fe_3O_4 loading. Oleic acid used as a co-surfactant to disperse nanoparticles in the fluid plays an important role in dynamic viscosity reduction and likely surface tension of nanofluids at 253.15K. Finally, based on these results, it can be envisaged to use these Fe_3O_4 nanofluids for cooling applications.

Acknowledgements

AB acknowledges EU COST for the STSM grant ref. COST-STSM-CA15119-42469 linked to the Cost Action “Overcoming Barriers to Nanofluids Market Uptake (NANOUPTAKE)” and for financial support in the participation of the 1st International Conference on Nanofluids (ICNf) and the 2nd European Symposium on Nanofluids (ESNf) held at the University of Castellón, Spain during 26–28 June 2019. PE acknowledges the European Union through the European Regional Development Fund (ERDF), the Ministry of Higher Education and Research, the French region of Brittany and Rennes Métropole for the financial support of both surface tension and thermal conductivity experimental devices.

References

[1] S.U.S. Choi, Enhancing thermal conductivity of fluids with nanoparticles., in: D.A.S.a.H.P. Wang. (Ed.) ASME International Mechanical Engineering Congress and Exposition Proceedings, ASME, San Francisco, CA,, 1995.
[2] R. Saidur, K.Y. Leong, H.A. Mohammad, A review on applications and challenges of nanofluids, Renewable and Sustainable Energy Reviews, 15(3) (2011) 1646-1668.
[3] H. Akoh, Tsukasaki, Y., Yatsuya, S., Tasaki, A. , Magnetic properties of ferromagnetic ultrafine particles prepared by vacuum evaporation on running oil substrate, Journal of Crystal Growth. , 45 (1978) 495–500.
[4] M.M. Rahman, S.S. Shevade, E. Ojada, Convective heat transfer in a composite trapezoidal microchannel during magnetic heating, International Communications in Heat and Mass Transfer, 37(9) (2010) 1175–1181.
[5] D. Kirby, J. Siegrist, G. Kijanka, L. Zavattoni, O. Sheils, J. O'Leary, R. Burger, J. Ducrée, Centrifugo-magnetophoretic particle separation. , Microfluidics and Nanofluidics, 13(6) (2012) 899–908.
[6] Q. Li, Y. Xuan, J. Wang, Experimental investigations on transport properties of magnetic fluids, Experimental Thermal and Fluid Science, 30(2) (2005) 109-116.
[7] H. Zhu, C. Zhang, S. Liu, Y. Tang, Y. Yin, Effects of nanoparticle clustering and alignment on thermal conductivities of Fe3O4 aqueous nanofluids, Applied Physics Letters, 89(2) (2006) 023123.
[8] G. Sekrani, S. Poncet, Ethylene- and Propylene-Glycol Based Nanofluids: A Litterature Review on Their Thermophysical Properties and Thermal Performances, Applied Sciences 8(11) (2018) 2311-2318.
[9] B. Aladag, S. Halelfadl, N. Doner, T. Maré, S. Duret, P. Estellé, Experimental investigations of the viscosity of nanofluids at low temperatures, Applied Energy, 97 (2012) 876-880.
[10] S. Halelfadl, P. Estellé, B. Aladag, N. Doner, T. Maré, Viscosity of carbon nanotubes water-based nanofluids: Influence of concentration and temperature, International Journal of Thermal Sciences, 71 (2013) 111-117.
[11] P.K. Namburu, D.P. Kulkarni, D. Misra, D.K. Das, Viscosity of copper oxide nanoparticles dispersed in ethylene glycol and water mixture, Experimental Thermal and Fluid Science, 32(2) (2007) 397-402.
[12] D.P. Kulkarni, D.K. Das, R.S. Vajjha, Application of nanofluids in heating buildings and reducing pollution., Applied Energy, 86(12) (2009) 2566-2573.
[13] D.P. Kulkarni, D.K. Das, G.A. Chukwu, Temperature dependent rheological property of copper oxide nanoparticles suspension (nanofluid), J Nanosci Nanotechnol, 6(4) (2006) 1150-1154.
[14] M.T. Naik, G.R. Janardhana, K.V.K. Reddy, B.S. Reddy, Experimental investigation into rheological property of copper oxide nanoparticles suspended in propylene glycol-water based fluids, Journal of Engineering and Applied Sciences, 5(6) (2010) 29–34.
[15] S.Z. Guo, Y. Li, J.S. Jiang, H.Q. Xie, Nanofluids Containing gamma-Fe_2O_3 Nanoparticles and their Heat Transfer Enhancements, Nanoscale Res Lett, 5(7) (2010) 1222-1227.
[16] L.S. Sundar, E.V. Ramana, M.K. Singh, A.C.M. De Sousa, Viscosity of low volume concentrations of magnetic Fe_3O_4 nanoparticles dispersed in ethylene glycol and water mixture, Chemical Physics Letters, 554 (2012) 236-242.
[17] M.T. Naik, L.S. Sundar, Investigation into Thermophysical Properties of Glycol based CuO Nanofluids for Heat Transfer Applications, World Academy of Science, Engineering and Technology, 59 (2011) 440-446.
[18] L.S. Sundar, E.V. Ramana, M.K. Singh, J. Gracio, A.C.M. Sousa, Preparation, Thermal and Rheological Properties of Propylene Glycol and Water Mixture Based Fe_3O_4 Nanofluids., Journal of Nanofluids, 3 (3) (2014) 200-209.
[19] K. Yapici, N.K. Cakmak, N. Ilhan, Y. Uludag, Rheological characterization of polyethylene glycol based TiO_2 nanofluids, Korea-Australia Rheology Journal, 26 (4) (2014) 355-363.

[20] A. Banisharif;, S.H. Elahi;, A.A. Firooz;, A.A. Khodadadi;, Y. Mortazavi;, TiO_2/Fe_3O_4 Nanocomposite Photocatalysts for Enhanced Photo-Decolorization of Congo Red Dye, Int. J. Nanosci. Nanotechnol., 9 (2013) 193-202.
[21] D. Cabaleiro, P. Estellé, H. Navas, A. Desforges, B. Vigolo, Dynamic Viscosity and Surface Tension of Stable Graphene Oxide and Reduced Graphene Oxide Aqueous Nanofluids, Journal of Nanofluids, 7(6) (2018) 1081-1088.
[22] ASHRAE Handbook 2009 Fundamentals, Physical Properties of Secondary Coolants, Atlanta, 2009.
[23] G. Żyła, J. Fal, P. Estellé, Thermophysical and dielectric profiles of ethylene glycol based titanium nitride (TiN–EG) nanofluids with various size of particles, International Journal of Heat and Mass Transfer, 113 (2017) 1189-1199.
[24] A. Banisharif, A.A. Khodadadi, Y. Mortazavi, A. Anaraki Firooz, J. Beheshtian, S. Agah, S. Menbari, Highly active Fe_2O_3-doped TiO_2 photocatalyst for degradation of trichloroethylene in air under UV and visible light irradiation: Experimental and computational studies, Applied Catalysis B: Environmental, 165 (2015) 209-221.
[25] S. Kiani, S.E. Rogers, M. Sagisaka, S. Alexander, A.R. Barron, A New Class of Low Surface Energy Anionic Surfactant for Enhanced Oil Recovery, Energy & Fuels, 33(4) (2019) 3162-3175.
[26] D.R.C. Lide, Handbook of Chemistry and Physics CRC Press, Taylor & Francis, Boca Raton, 2005-2006.
[27] Nadia Salih, Jumat Salimon, E. Yousif, The physicochemical and tribological properties of oleic acid based triester biolubricants, Industrial Crops and Products, 34(1) (2011) 1089-1096.
[28] S. Reaume, N. Ellis, Use of Isomerization and Hydroisomerization Reactions to Improve the Cold Flow Properties of Vegetable Oil Based Biodiesel, Energies, 6(2) (2013) 619-633.
[29] Nadia Salih, Jumat Salimon, E. Yousif, The Effect Of Chemical Structure On Pour Point, Oxidative Stability And Tribological Properties Of Oleic Acid Triester Derivatives, he Malaysian Journal of Analytical Sciences, 17 (2013) 119 - 128.
[30] J. Yang, H. Yan, Z. Hu, D. Ding, Viscosity and sedimentation behaviors of the magnetorheological suspensions with oleic acid/dimer acid as surfactants, Journal of Magnetism and Magnetic Materials, 417 (2016) 214-221.
[31] S.M.S. Murshed, P. Estellé, A state of the art review on viscosity of nanofluids, Renewable and Sustainable Energy Reviews, 76 (2017) 1134-1152.
[32] D.P. Kulkarni, D.K. Das, G.A. Chukwu, Temperature Dependent Rheological Property of Copper Oxide Nanoparticles Suspension (Nanofluid), Journal of Nanoscience and Nanotechnology, 6(4) (2006) 1150-1154.
[33] R. Gómez-Villarejo, T. Aguilar, S. Hamze, P. Estellé, J. Navas, Experimental analysis of water-based nanofluids using boron nitride nanotubes with improved thermal properties, Journal of Molecular Liquids, 277 (2019) 93-103.
[34] T.X. Phuoc, M. Massoudi, R.-H. Chen, Viscosity and thermal conductivity of nanofluids containing multi-walled carbon nanotubes stabilized by chitosan, International Journal of Thermal Sciences, 50(1) (2011) 12-18.
[35] L. Chen, H. Xie, W. Yu, Y. Li, Rheological Behaviors of Nanofluids Containing Multi-Walled Carbon Nanotube, Journal of Dispersion Science and Technology, 32(4) (2011) 550-554.
[36] J. Philip, P.D. Shima, Thermal properties of nanofluids, Advances in colloid and interface science, 183-184 (2012,) 30–45.
[37] D.S. Wen, G. Lin, S. Vafaei, K. Zhang, Review of nanofluids for heat transfer applications, Particuology, 7 (2) (2009) 141-150.
[38] M. Shanbedi, A. Amiri, S. Heris, S. Kazi, C. Teng, Nanofluids: Basic Principles and Modern Aspects, in: In CRC Concise Encyclopedia of Nanotechnology, CRC Press, 2015, pp. 724-768.
[39] S. Simpson, A. Schelfhout, C. Golden, S. Vafaei, Nanofluid Thermal Conductivity and Effective Parameters, Applied Sciences, 9(87) (2018) 1-56.

[40] A. Ghadimi, R. Saidur, H.S.C. Metselaar, A review of nanofluid stability properties and characterization in stationary conditions, International Journal of Heat and Mass Transfer, 54 (17-18) (2011) 4051-4068.
[41] O. Mahian, L. Kolsi, M. Amani, P. Estellé, G. Ahmadi, C. Kleinstreuer, J.S. Marshall, M. Siavashi, R.A. Taylor, H. Niazmand, S. Wongwises, T. Hayat, A. Kolanjiyil, A. Kasaeian, I. Pop, Recent advances in modeling and simulation of nanofluid flows-Part I: Fundamentals and theory, Physics Reports, 790 (2019) 1-48.
[42] L. Qiu, N. Zhu, Y. Feng, E.E. Michaelides, G. Żyła, D. Jing, X. Zhang, P.M. Norris, C.N. Markides, O. Mahian, A review of recent advances in thermophysical properties at the nanoscale: From solid state to colloids, Physics Reports, (2019).
[43] S. Babita, G.S. M., Preparation and evaluation of stable nanofluids for heat transfer application: A review, Experimental Thermal and Fluid Science, 79 (2016) 202–212.
[44] L. Blaney, Magnetite (Fe_3O_4): Properties, Synthesis, and Applications, in: In Lehigh Review, , Lehigh Preserve, 2007.
[45] K.K. Varma, P. Kishore, P.D. Prasad, Enhancement of Heat Transfer Using Fe3O4/Water Nanofluid with Varying Cut-Radius Twisted Tape Inserts, International Journal of Applied Engineering Research, 12(18) (2017) 7088-7095.
[46] W. Yu, S.U.S. Choi, The Role of Interfacial Layers in the Enhanced Thermal Conductivity of Nanofluids: A Renovated Maxwell Model, Journal of Nanoparticle Research, 5(1) (2003) 167-171.
[47] R. Prasher, P.E. Phelan, P. Bhattacharya, Effect of aggregation kinetics on the thermal conductivity of nanoscale colloidal solutions (nanofluid), Nano letters, 6(7) (2006) 1529-1534.
[48] W. Evans, R. Prasher, J. Fish, P. Meakin, P. Phelan, P. Keblinski, Effect of aggregation and interfacial thermal resistance on thermal conductivity of nanocomposites and colloidal nanofluids, International Journal of Heat and Mass Transfer, 51(5-6) (2008) 1431-1438.
[49] R. Prasher, P. Bhattacharya, P.E. Phelan, Thermal conductivity of nanoscale colloidal solutions (nanofluids), Physical review letters, 94(2) (2005) 025901.
[50] C. Pang, J.-Y. Jung, Y.T. Kang, Aggregation based model for heat conduction mechanism in nanofluids, International Journal of Heat and Mass Transfer, 72 (2014) 392-399.
[51] P. Estellé, D. Cabaleiro, G. Żyła, L. Lugo, S.M.S. Murshed, Current trends in surface tension and wetting behavior of nanofluids, Renewable and Sustainable Energy Reviews, 94 (2018) 931-944.
[52] M. Wanic, D. Cabaleiro, S. Hamze, J. Fal, P. Estellé, G. Żyła, Surface tension of ethylene glycol-based nanofluids containing various types of nitrides, Journal of Thermal Analysis and Calorimetry, (2019) 1-8.
[53] N. Berrada, S. Hamze, A. Desforges, J. Ghanbaja, J. Gleize, T. Mare, B. Vigolo, P. Estellé, Surface tension of functionalized MWCNT-based nanofluids in water and commercial propylene-glycol mixture, Journal of Molecular Liquids, 293 (2019) 111473.
[54] R. Gómez-Villarejo, P. Estellé, J. Navas, Boron nitride nanotubes-based nanofluids with enhanced thermal properties for use as heat transfer fluids in solar thermal applications, Solar Energy Materials and Solar Cells, 205 (2020) 110266
[55] P. Martínez-Merino, S. D. Midgley, E. I. Martín, P. Estellé, R. Alcántara, A. Sánchez-Coronilla, R. Grau-Crespo, J. Navas, Novel WS2-Based Nanofluids for Concentrating Solar Power: Performance Characterization and Molecular-Level Insights, ACS Applied Materials & Interfaces (2020) Article ASAP, DOI: 10.1021/acsami.9b18868
[56] N.M. van Os, J.R. Haak, L.A.M. Rupert, Physico-chemical properties of selected anionic, cationic and nonionic surfactants, Elsevier, 2012.
[57] J. Drelich, Ch. Fang, C.L. White, Measurement of interfacial tension in Fluid-Fluid System, Michigan Technological University,, Houghton, Michigan, 2002.
[58] L. Cheng, E.P. Bandarra Filho, J.R. Thome, Nanofluid Two-Phase Flow and Thermal Physics: A New Research Frontier of Nanotechnology and Its Challenges, Journal of Nanoscience and Nanotechnology, 8(7) (2008) 3315-3332.

[59] M. Radiom, C. Quan, C. Yang, K. Qian, A.K. Asundi, W.K. Chan, F.S. Chau, Characterization of surface tension and contact angle of nanofluids, in: Fourth International Conference on Experimental Mechanics, 2009.

Nomenclature

T	Temperature [K]
W	Water
EG	Ethylene Glycol
SDS	Sodium Dodecyl Sulfonate
OA	Oleic acid
ST	Surface Tension [mN/m]

Greek symbols

μ	Dynamic viscosity [Pa.s or mPa.s]
$\dot{\gamma}$	Shear rate [s^{-1}]
τ	Shear rate [Pa]
K or k	Thermal conductivity [$W.m^{-1}.K^{-1}$]
ρ	Density [kg/m^3]
ϕ	Volume fraction of nanoparticle

Subscripts

bf	Base fluid
nf	Nanofluid
np	Nanoparticle

Highlights

- Preparation and characterization of Fe_3O_4 water/ethylene glycol (50/50 in vol.%) based nanofluids
- Experimental investigation of thermal conductivity, dynamic viscosity and surface tension
- Influence of nanoparticle loading 0.01/0.1 %vol. and temperature 253.15-293.15K
- Enhanced properties relevant for cooling applications